Morphological instabilities of stressed and reactive geological interfaces

Luiza Angheluta, Joachim Mathiesen, Chaouqi Misbah, François Renard

JOURNAL OF GEOPHYSICAL RESEARCH, VOL. 115, B06406, doi:10.1029/2009JB006880, 2010

Morphological instabilities of stressed and reactive geological interfaces

Luiza Angheluta,[1] Joachim Mathiesen,[1,2] Chaouqi Misbah,[3] and François Renard[1,4]

Received 13 August 2009; revised 21 December 2009; accepted 20 January 2010; published 24 June 2010.

[1] Interfaces between contacting rocks of the Earth's crust are shown to be unstable and corrugating and develop roughness at various scales when submitted to nonhydrostatic stress. This instability may occur in various geological settings as long as a coherent deformation of the interface is allowed and the bodies that the interface separates have different material properties (i.e., viscosity, density, or elastic moduli). Relevant examples include fault planes, dissolution interfaces, or grain boundaries. Performing a two-dimensional linear stability analysis, we consider two cases: one solid in contact with a viscous layer and two solids separated by a thin viscous layer. In both cases either shear and/or normal loads are imposed on the interface and thermodynamical conditions for the initiation of roughening are established. Applied on several geological systems such as grain contacts and fault planes, we propose that our analysis can explain how complex patterns may emerge at rock-rock interfaces. Finally, we provide an analysis of the evolution of the static friction coefficient along sheared interfaces. The evolution is shown to depend solely on Poisson's ratio of the solid and the ratio of the shear and compressional stresses along the interface.

Citation: Angheluta, L., J. Mathiesen, C. Misbah, and F. Renard (2010), Morphological instabilities of stressed and reactive geological interfaces, *J. Geophys. Res.*, *115*, B06406, doi:10.1029/2009JB006880.

1. Introduction

[2] In the rocks of the Earth's crust, interfaces between stressed solids with different material properties are ubiquitous at all scales; grain-grain contacts, interfaces between sedimentary layers, dissolution interfaces (i.e., pressure solution seams and stylolites), and fault mirrors are well-known examples. It is also known, now for more than 30 years in the geophysics community, that solid-solid or solid-liquid interfaces can become morphologically unstable when submitted to deviatoric stresses. Such instability has been described theoretically for coherent grain-grain contacts [*Fletcher*, 1973], for liquid-crystals interfaces [*Misbah et al.*, 2004], or for stylolites [*Schmittbuhl et al.*, 2004; *Koehn et al.*, 2007]; see also Figure 1. The nonequilibrium thermodynamics of mass transport by intracrystalline diffusion under nonhydrostatic stress has been considered in a number of works [*Shimizu*, 1997; *Ghoussoub and Leroy*, 2001]. Moreover, roughness instability of stressed solids has also been observed in laboratory experiments on salt crystals [*den Brok and Morel*, 2001; *Dysthe et al.*, 2003; *de Meer et al.*, 2005; *Bisschop and Dysthe*, 2006; *van Noort et al.*, 2007] and in helium crystals [*Torii and Balibar*, 1992].

[3] In the physics community, the morphological stability of material interfaces is also widely studied. It has been proposed that the interface between a solid and its melt is unstable when the solid is nonhydrostatically loaded [*Asaro and Tiller*, 1972; *Grinfeld*, 1986, 1992; *Misbah et al.*, 2004]. The surface of a solid in contact with its solution corrugates and develops parallel grooves when the solid is stressed. The instability is controlled by a competition between mechanical forces that favor a roughening of the interface and a stabilizing force due to surface tension. In cases of relatively low surface tension, the grooves may in a nonlinear regime concentrate large stresses and lead to crack nucleation [*Yang and Srolovitz*, 1993; *Kassner and Misbah*, 1994]. Obviously, the interface grooves and micro-crack formation can strongly modify the mechanical properties of the solid. More recently, it has been shown that for solid-solid interfaces a similar instability is triggered by a finite jump in the free energy density across the interface and that the instability leads to the formation of fingerlike structures aligned with the principal direction of compressive stresses [*Angheluta et al.*, 2008]. The instability turns out to be very sensitive to small variations in density and elastic parameters (in particular Poisson's ratio) across the interface of the two solids [*Angheluta et al.*, 2009].

[4] A rich morphology or roughness, universal to most fracture surfaces, is also observed on fault planes. The characteristic scale-free roughness of faults is often ascribed

[1]Physics of Geological Processes, University of Oslo, Blindern, Norway.
[2]Also at Niels Bohr Institute, University of Copenhagen, Denmark.
[3]Laboratoire de Spectrométrie Physique, University Joseph Fourier, Grenoble I, CNRS, Grenoble, France.
[4]Also at Observatoire des Sciences de l'Univers de Grenoble, Laboratoire de Géodynamique des Chaînes Alpines, University Joseph Fourier, Grenoble I, CNRS, Grenoble, France.

0148-0227/10/2009JB006880

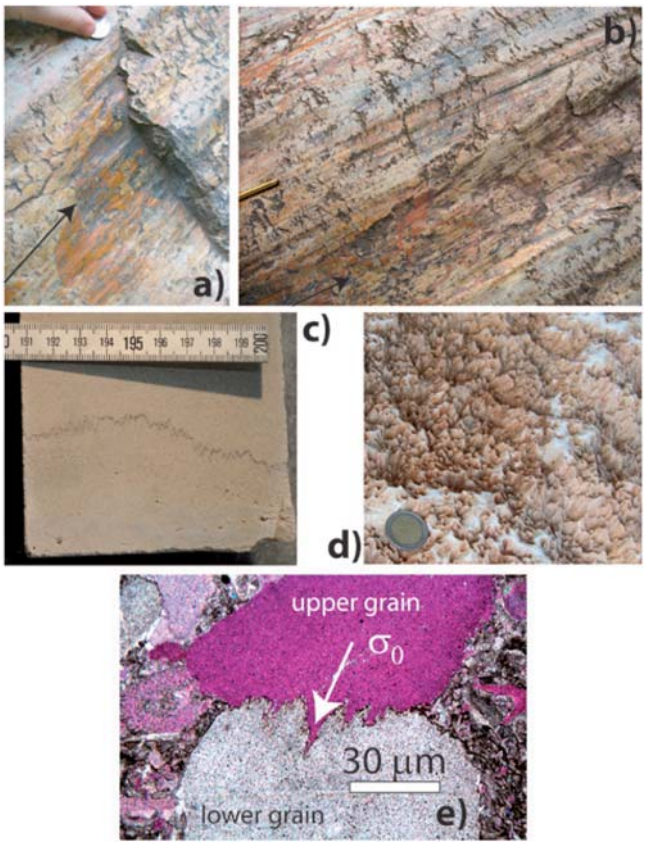

Figure 1. Geological rough interfaces. (a and b) Fault surface in cherts showing small-scale striations (Corona Heights Fault, San Francisco, California). (a) Coin or (b) pen are shown for scales. (c) Stylolite interface in marl from the Kimmeridgian limestones in the Paris Basin. (d) Three-dimensional view of a stylolite in limestone (coin for scale), Northern Israel. (e) Grain-grains rough interface in a limestone from Mons, Belgium.

to mechanical abrasion and fault branching following from the cycles of abrupt slip and arrest [*Power et al.*, 1987, 1988; *Ben Zion and Sammis*, 2003; *Renard et al.*, 2006; *Sagy et al.*, 2007]. Moreover, along some faults a slow aseismic creep is observed (for a review on slow earthquakes, see *Schwartz and Rokosky* [2007]; for a review on postseismic slip, see *Pritchard and Simons* [2006]), indicating that the motion of the fault somehow overcomes the roughness of asperities on the fault surface. One possible explanation for this nontrivial rheology could be the presence of a stress-controlled dissolution-precipitation alteration of the contact surface. In general, reactive fluids are present at the fault plane and act as a medium that accommodates the dissolution of asperities in regions of high stress and possible precipitation in regions of low stress [*Gratier et al.*, 2003]. The dissolution-precipitation processes may modify the morphology and may invoke an effective creep deformation where the external loading is dissipated through small-scale alteration. Finally, such processes, when occurring at the grain scale, may have an effect on the attenuation of seismic waves [*Ricard et al.*, 2009].

[5] We shall here consider geological systems where mass diffuses along a sharp interface by dissolution-precipitation or other transport mechanisms. The rate of mass transfer is determined from the chemical potential of a single soluble component. We consider two-dimensional (2-D) model systems (see Figure 2) composed of either a linear elastic solid in contact with a viscous liquid or two solid bodies separated by a thin viscous interface. Stresses applied to both types of systems far away from the interface give rise to morphological alterations at the surface(s) of the solid phase(s). In the solid-liquid system, one elastic solid occupies the lower region $y < h(x, t)$, where $h(x, t)$ represents the interface profile as shown in Figure 2 and is in contact with an incompressible fluid extending over the upper region. Both model cases are analyzed below using various boundary conditions. When two solids are in contact through a thin fluid film we impose a normal load that balances the hydrostatic fluid pressure at the interface. For a static fluid, the limit of zero thickness for the fluid layer is well defined and, in that limit, the effect of fluid is through the force balance conditions at the interface. In the case of a liquid-solid interface, we study the nonequilibrium response due to a uniform shear stress τ_0 and compressional load σ_0. In the absence of applied forces, the solid is assumed to be in chemical and mechanical equilibrium with a fluid phase at hydrostatic pressure P_0.

[6] We perform a stability analysis in 2-D by first calculating the chemical potential along a flat interface in a mechanically loaded system. Then we deform the interface (keeping the system loaded) by a small size perturbation and calculate by an expansion in the height the corresponding change in chemical potential. Finally, based on the chemical potential we derive amplitude equations that determine if an

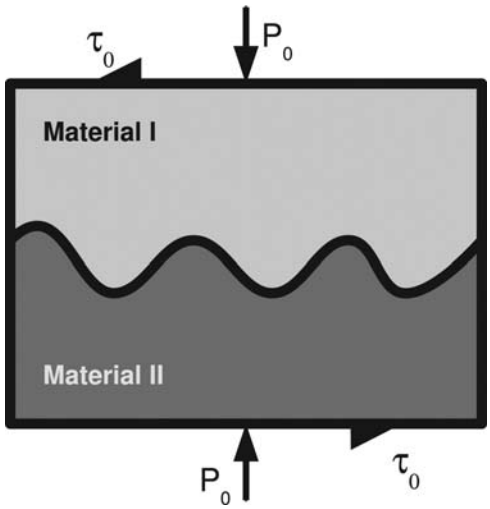

Figure 2. Model setup for geological interfaces. Two materials, with different properties, either both elastic with different parameters (elastic, density) or one elastic solid and one viscous layer. This latter setup could correspond to a fault zone, with a viscoelastic core and an elastic damaged zone. A compressional or shear force is applied at the margins in the vertical direction. We will consider several cases: either the interface has a negligible thickness (corresponding to e.g., a fracture, dissolution seam, grain boundary) or the interface has a finite thickness and contains a viscous material (e.g., stylolites or a fault zone).

instability is thermodynamically favored. Such an analysis provides a thermodynamic criteria for the development of roughness or for the flattening of the interface.

2. Chemical Potential of a Stressed Interface

[7] When a stressed solid is in contact with a saturated solution, the change in chemical potential at the interface equals the work required to move a soluble component from a stressed configuration to a hydrostatic configuration [*Paterson*, 1973; *Sekerka and Cahn*, 2004]

$$\mu[x, h(x,t)] = \mathcal{F}(x, h(x,t))\mathcal{V}_0 - \sigma_{nn}[x, h(x,t)](\mathcal{V} - \mathcal{V}_0) + \kappa\gamma\mathcal{V}_0, \tag{1}$$

where γ is the surface tension and $h(x, t)$ is the interface height or the vertical coordinate on Figure 2. The curvature is taken to be positive for a concave interface $\kappa = -h''(1 + h'^2)^{-3/2}$, where $h' = \partial_x h(x, t)$. $\mathcal{V} - \mathcal{V}_0$ is the change in molar volume across the interface. For simplicity, we assume that at equilibrium the component in the solid phase has the same molar volume $\mathcal{V}_0$ as in the fluid phase. Thus, in the stressed configuration the molar volume changes due to elastic volumetric expansion or contraction, i.e., $\mathcal{V} = \mathcal{V}_0(1 + \epsilon_{kk})$, where ϵ_{kk} is the trace of the elastic strains (summation over repeating indices is implied). $\mathcal{F}$ is the Helmholtz free energy per unit volume, and σ_{nn} is the normal component of the stress vector. For a free surface $\sigma_{nn} = 0$, while if the surface is in contact with a fluid (gas, aqueous liquid, melt), then $\sigma_{nn} = -p$ with p being the hydrostatic pressure in the fluid.

[8] The surface gradients in the chemical potential produce a drift of surface atoms with a flux given by *Mullins* [1957]

$$J = -\frac{D_s}{kT\mathcal{V}_0}\frac{\partial \mu}{\partial s}, \tag{2}$$

where D_s is the surface diffusion coefficient and kT is the Boltzmann's constant times temperature and s is the interfacial arc length. Note here that, depending on the system, D_s could represent diffusion along the solid surface (Coble creep) or along a thin water film located at the interface (dissolution precipitation creep); in both cases the existence of an instability does not depend on the transport mechanism [*Misbah et al.*, 2004], but the kinetics of the process does. The divergence of the mass flux gives the change in the number of atoms per unit area per unit time and can be directly related to the normal velocity of the interface via

$$V_n = -\mathcal{V}_0 a^2 \frac{\partial J}{\partial s} = M\frac{\partial^2 \mu}{\partial s^2}, \tag{3}$$

where a is the surface density of atoms and $M = D_s a\mathcal{V}_0/kT$ is a positive mobility coefficient.

[9] For small morphological perturbations [i.e., $h(x, t) \ll 1$], the time derivative of $h(x, t)$ is given by the normal velocity, and the spacial derivative along the interface arc is approximated by the x derivative. There, we have that

$$\frac{\partial h(x,t)}{\partial t} = M\frac{\partial^2 \mu[h(x,t)]}{\partial x^2}. \tag{4}$$

The above equation describes the morphological evolution of the interface due to mass transport by diffusion. A linear stability analysis was carried out for free surfaces in [*Srolovitz*, 1989], as well as for surfaces in contact with a hydrostatic fluid [*Gal et al.*, 1998; *Cantat et al.*, 1998], where the solid was stressed on the lateral boundaries normal to the interface. The nonlinear morphological evolution leads to cusplike singularities in finite time [*Yang and Srolovitz*, 1993; *Xiang and E.*, 2002]. These previous analyses considered systems where normal forces are present at the interface but did not consider the effect of shear forces.

3. Interface Between a Solid and a Viscous Layer Under Nonhydrostatic Shear Stress

3.1. Definition of the Equilibrium Configuration

[10] Under the assumption that the system is instantaneously relaxing to its equilibrium configuration, we consider the steady state of the momentum equations both for the elastic solid and the viscous fluid. In the solid phase the stress of an elastostatic two-dimensional configuration is conveniently solved in terms of the Airy stress function, $U(x, y)$ [*Muskhelishvili*, 1953], which satisfies the bi-Laplace equation $\Delta^2 U = 0$. We have here introduced the Laplace operator $\Delta = \frac{\partial^2}{\partial x^2} + \frac{\partial^2}{\partial y^2}$. Once the stress function has been found, the stress tensor components readily follow from the relations

$$\sigma_{xx} = \frac{\partial^2 U}{\partial y^2}, \quad \sigma_{yy} = \frac{\partial^2 U}{\partial x^2}, \quad \sigma_{xy} = -\frac{\partial U}{\partial x \partial y}. \tag{5}$$

The viscous flow is described in terms of Stokes' equation. That is, away from the interface, the combined equations for the viscous layer and solid take the form

$$\Delta^2 U(x,y) = 0, \ \mu\Delta\mathbf{w} - \nabla p(x,y) = 0, \ \nabla \cdot \mathbf{w} = 0, \tag{6}$$

where $p(x, y)$ is the pressure in the viscous layer, and $\mathbf{w}(x, y)$ is the velocity vector field of the viscous layer with components $\mathbf{w} = (u, v)$. The second equation relates the velocity in the viscous layer to the pressure gradient. The last equation represents the continuity of the velocity field in the viscous layer. Note that the equations are not directly coupled, however, in the following, we shall introduce a coupling of the equations via the boundary conditions. That is the phases interact only at their boundaries.

[11] At the fluid-solid interface, we require force balance and a no-slip condition formalized in the following relations

$$\sigma_{nn} = -p + 2\mu\partial_n w_n, \ \sigma_{nt} = \mu(\partial_n w_t + \partial_t w_n),$$
$$w_n = 0, \ w_t = 0, \tag{7}$$

where $(n_x, n_y) \approx (-\partial_x h, 1)$ is the local unit vector pointing into the viscous phase and $(t_x, t_y) \approx (1, \partial_x h)$ is the tangent vector, in the limit where the interface amplitude is small enough. The surface tension effect on the normal stress vector has a contribution that is smaller than the surface energy, and thus, for the sake of simplicity, we have neglected it.

[12] In addition, we need to specify the far-field boundary conditions. We study the linear response away from the hydrostatic configuration in the presence of an applied

compressional load σ_0 and shear stress τ_0 as sketched in Figure 2. In a more general formalism than the Asaro-Tiller-Grinfled instability [*Asaro and Tiller*, 1972; *Grinfeld*, 1986], we allow the fluid to flow at a constant shear rate, τ_0.

3.2. Flat Interface

[13] For a flat interface [i.e., $h(x, t) = 0$], the viscous flow is decoupled from the elastic deformations and the solution is the same as for a flow past a planar wall, namely

$$u^{(0)}(x,y) = \frac{\tau_0}{\mu} y,\ v^{(0)}(x,y) = 0,\ p^{(0)}(x,y) = P_0, \tag{8}$$

where the upper index refers to the order of the morphological perturbation expansion. From the force balance at the interface and the far-field applied load, we can determine the stress components as given by

$$\sigma^{(0)}_{yy}(x,y) = -P_0, \tag{9}$$

$$\sigma^{(0)}_{xy}(x,y) = \tau_0, \tag{10}$$

$$\sigma^{(0)}_{xx}(x,y) = -P_0 + \sigma_0, \tag{11}$$

and the Airy's stress function is given as

$$U^{(0)}(x,y) = -P_0 \frac{x^2}{2} + (\sigma_0 - P_0)\frac{y^2}{2} - \tau_0 xy. \tag{12}$$

The constant stress field implies a constant chemical potential along the interface. In the absence of gradients, no mass diffusion will occur. However, when the interface has a nonzero curvature, the stress vector and the elastic energy vary along the interface and induce mass transport.

3.3. Perturbed Interface

[14] For an undulating interface, the field variables are in general altered from their counterparts around a flat interface. We consider a small amplitude perturbation on the form $h(x, t) = \epsilon h^{(1)}(x, t)$, where $\epsilon \ll 1$ is the expansion parameter and $h^{(1)}(x, t)$ is the first order correction to a flat interface. A field variable $F(x, y)$, which is a solution to the perturbed interface, can be expanded to the leading order in terms of the solution to a flat interface as follows:

$$F(x,y) = F^{(0)}(x,y) + \epsilon F^{(1)}(x,y) + \mathcal{O}(\epsilon^2), \tag{13}$$

where $F(x, y)$ denotes any of the field variables, $U(x, y)$, $p(x, y)$, $u(x, y)$, $v(x, y)$. $F^{(0)}(x, y)$ is the solution to a planar interface, and $F^{(1)}(x, y)$ is a first order correction due to a shape perturbation. Evaluated at a point on the interface $y = \epsilon h^{(1)}(x, t)$, the expansion becomes

$$F(x, \epsilon h^{(1)}) = F^{(0)}(x,0) + \epsilon h^{(1)} \partial_y F^{(0)}(x,y)|_{y=0} + \epsilon F^{(1)}(x,0) + \mathcal{O}(\epsilon^2).$$

For example, the stress at the interface is evaluated by expanding around its constant value at a planar interface

$$\sigma_{ij}(x, \epsilon h^{(1)}) = \sigma^{(0)}_{ij}(x,0) + \epsilon \sigma^{(1)}_{ij}(x,0) + \mathcal{O}(\epsilon^2). \tag{14}$$

Inserting these perturbations into the interfacial conditions from equations (7) and retaining the first order terms, we obtain the following relations

$$\begin{aligned}
&\sigma^{(1)}_{yy}(x,0) = -p^{(1)}(x,0) + 2\mu \partial_y v^{(1)}(x,0),\\
&\sigma^{(1)}_{xy}(x,0) = \mu\left[\partial_x v^{(1)}(x,0) + \partial_y u^{(1)}(x,0)\right],\\
&v^{(1)}(x,0) = 0,\\
&u^{(1)}(x,0) = -h^{(1)}\frac{\tau_0}{\mu}.
\end{aligned} \tag{15}$$

The linear perturbation fields are determined from equations (6) combined with the above state interfacial conditions. The far-field boundary conditions are satisfied by the zeroth-order terms, thus we require that the perturbations decay to zero at infinity. Assuming periodic boundary conditions along the x axis, we can decompose the interface amplitude and the field perturbations into a superposition of Fourier modes as $h^{(1)}(x, t) = \int dk h^{(1)}_k(t) e^{ikx}$ and $F^{(1)}(x, y) = \int dk F^{(1)}_k(y) e^{ikx}$. Solving the governing set of equations combined with the interfacial boundary conditions in the Fourier space, we obtain the following solutions

$$U^{(1)}_k(y) = h^{(1)}_k[(-\sigma_0 + 2i\tau_0)y]e^{ky}, \tag{16}$$

$$p^{(1)}_k(y) = 2ih^{(1)}_k \tau_0 k e^{-ky}, \tag{17}$$

$$u^{(1)}_k(y) = \frac{h^{(1)}_k \tau_0 (ky - 1)}{\mu} e^{-ky}, \tag{18}$$

$$v^{(1)}_k(y) = \frac{ih^{(1)}_k \tau_0}{\mu} k y e^{-ky}. \tag{19}$$

The fields are computed in the real space by integrating up all the Fourier modes,

$$F(x,y) = F^{(0)}(x,y) + \epsilon \int dk F^{(1)}_k(y) e^{ikx}. \tag{20}$$

However, in the linear regime, the modes are decoupled, and therefore it is possible to study their stability independently.

3.4. Stability Analysis

[15] We can now return to the evolution of a morphological perturbation by mass diffusion along a chemical potential gradient as in equation (4), where

$$\mu^{(1)}(x,0) = \left(\mathcal{F}^{(1)} - \sigma^{(1)}_{nn}\epsilon^{(0)}_{kk} - \sigma^{(0)}_{nn}\epsilon^{(1)}_{nn} - \gamma \partial_x^2 h^{(1)}\right)\mathcal{V}_0. \tag{21}$$

From the definition of the Airy's stress function given in equation (16) we determine the perturbation stresses required to evaluate the chemical potential at the interface by using equation (5). Hereby, we perform the calculations in the plane strain approximation. A similar analysis can be performed in the plane stress limit.

[16] We consider an isothermal mass diffusion process such that the Helmholtz free energy is determined by the elastic energy of deformation, which is defined as

$$\mathcal{F}(x,y) = \frac{1}{4G}\left[(1-\nu)(\sigma^2_{xx} + \sigma^2_{yy}) - 2\nu\sigma_{xx}\sigma_{yy} + 2\sigma^2_{xy}\right], \tag{22}$$

where G is the shear modulus and ν is the Poisson's ratio. The elastic strain energy is a superposition of the reference energy associated with a planar interface and the energy due to a morphological perturbation

$$\mathcal{F}(x, \epsilon h) = \mathcal{F}^{(0)}(x, 0) + \epsilon \mathcal{F}^{(1)}(x, 0), \tag{23}$$

where

$$\mathcal{F}^{(0)} = \frac{(1-\nu)\sigma_0^2 + 2\tau_0^2 - 2(1-2\nu)(\sigma_0 - P_0)P_0}{4G},$$

$$\mathcal{F}^{(1)} = \frac{1}{2G}\Big\{[(1-\nu)\sigma_0 + 2\nu P_0]\sigma_{xx}^{(1)} - [\nu\sigma_0 + (1-2\nu)P_0]\sigma_{yy}^{(1)} + 2\tau_0\sigma_{xy}^{(1)}\Big\}.$$

The normal stress vector in the solid phase is expanded as

$$\sigma_{nn}(x, 0) = -P_0 + \epsilon\Big[\sigma_{yy}^{(1)}(x, 0) - 2\tau_0\partial_x h^{(1)}\Big]. \tag{24}$$

Also, the volumetric change expressed by the trace of the strain field is related to stresses as follows,

$$\epsilon_{kk} = \frac{1-2\nu}{2G}(\sigma_{xx} + \sigma_{yy}) = \frac{1-2\nu}{2G} \cdot \Big[(\sigma_0 - 2P_0) + \epsilon\Big(\sigma_{xx}^{(1)} + \sigma_{yy}^{(1)}\Big)\Big].$$

Now, inserting these expressions into equation (21) and decomposing the linear perturbation of the chemical potential into a superposition of Fourier modes as $\mu(x, 0) = \int dk\, \mu_k^{(1)} e^{ikx}$, where k is an arbitrary wave number, we obtain that the Fourier coefficient $\mu_k^{(1)}$ is given by

$$\mu_k^{(1)} = \alpha + i\beta, \tag{25}$$

where

$$\alpha = -\frac{(1-\nu)\sigma_0^2 - 2\tau_0^2}{G} kh_k^{(1)} + k^2 h_k^{(1)}\gamma$$

$$\beta = \frac{-2(1-2\nu)\tau_0 P_0 + 4(1-\nu)\tau_0\sigma_0}{G} kh_k^{(1)}.$$

For an exponential growth $h_k^{(1)} = \exp(\omega t)$, the linearized interfacial dynamics from equation (4) reduces to a dispersion relation $\omega = \omega(k)$. The morphological stability is determined from the sign of the real part of the growth rate, which is given by

$$\Re(\omega) = M\mathcal{V}_0\left[\frac{(1-\nu)\sigma_0^2 - 2\tau_0^2}{G}k^3 - k^4\gamma\right]. \tag{26}$$

There exists a crossover in stability at a finite wave number k_c given by

$$k_c = \frac{(1-\nu)\sigma_0^2 - 2\tau_0^2}{G\gamma}, \tag{27}$$

when the applied stresses satisfy the inequality

$$(1-\nu)\sigma_0^2 > 2\tau_0^2. \tag{28}$$

The interface is therefore predicted to be linearly unstable at wave numbers $k > k_c$. The shear stress adds an imaginary component, which may be related to waves, and a stabilizing term to the real part of the growth rate. In the absence of shear stress, the classical Asaro-Tiller-Grinfeld instability above a critical wave number $k_c = (1-\nu)\sigma_0^2/G\gamma$ is obtained.

[17] We have so far assumed no-slip conditions at the interface. The important question is then, if the morphological instability is present at shear loads close to the onset of slip. According to Coulomb's friction law, the critical shear stress of slip σ_{nt} is linearly proportional to the normal load $\sigma_{nt} = \mu_s\sigma_{nn}$, where μ_s is the static friction coefficient. For $\sigma_0 = P_0$ the elastic solid is effectively compressed by the fluid hydrostatic pressure in the normal direction to the interface. Hereby, the instability arises from the competition between the magnitude of the shear stress and the effective normal load (i.e., the interface is linearly unstable if the system is dominated by the pressure/normal load P_0 and stable if the shear stress τ_0 dominates). At the onset of slip, the stability criterion given in equation (28) with P_0 as an effective normal load is equivalent to

$$\mu_s < \sqrt{\frac{1-\nu}{2}}. \tag{29}$$

From this inequality, we see that the stability depends crucially on the value of Poisson's ratio. For rocks, Poisson's ratio is in the range [0.2–0.4], indicating that the transition to roughening instability should occur for $\mu_s <$ [0.5–0.6]. Note that when the system is unstable, the interface roughness grows rough in time and thereby the static friction coefficient increases, whereas when $\mu_s > \sqrt{\frac{1-\nu}{2}}$ the interface becomes less rough and the static friction coefficient should decrease.

4. Two Solid Materials Separated by a Thin Viscous Layer

[18] We now consider a system composed of a thin viscous layer at hydrostatic pressure P_0 sandwiched between two identical linearly elastic solids. In the absence of externally applied stresses, the solids are in equilibrium with each other and with the fluid film and the systems in hydrostatically stressed. We bring the system out of equilibrium by applying a compressional load σ_0 along the interface, and, in particular, for $\sigma_0 = P_0$, the solids effectively sustain a normal load from the fluid pressure. For a finite thickness one can study the case where the fluid film is flowing at a constant shear rate. However, the limit of zero thickness is singular, in the sense that the strain rate becomes infinite. For simplicity, we therefore assume that the fluid is at rest (i.e. $\tau_0 = 0$) and consider the limit where the fluid thickness is infinitely small compared to the size of the solid bodies (see Figure 2). In this case, the fluid film acts through the boundary condition at the solid-solid interface, by setting the tangential stress vector to zero and the normal stress vector equal to the hydrostatic pressure, namely

$$\sigma_{nn,j} = -P_0, \tag{30}$$

$$\sigma_{nt,j} = 0, \tag{31}$$

where $j = 1, 2$ is the phase index. One could also include the surface tension effects into the interface boundary conditions

without much difficulty. Under these conditions, a similar perturbation technique is carried out as in the previous section. The bi-Laplace equation is solved for each solid phase $j = 1, 2$ and the Airy's stress functions $U_j(x, y)$ are determined from the interfacial boundary conditions. The zeroth order solution associated with a flat interface is given by

$$U_j^{(1)} = -P_0 \frac{x^2}{2}, \tag{32}$$

and the linear order terms due to a small morphological perturbation $h(x, t) = \epsilon h^{(1)}(x, t)$ are obtained as

$$U_1^{(1)}(x,y) = -P_0 y e^{ky} h^{(1)}(x,t),\ U_2^{(1)}(x,y) = P_0 y e^{-ky} h^{(1)}(x,t). \tag{33}$$

The stress components are then evaluated by inserting the Airy's stress functions into equation (5). We find that the linear perturbation in the chemical potential calculated in the plane strain approximation, is given by

$$\mu(x,0) = \frac{1-\nu}{4G} P_0^2 - \epsilon \frac{1-\nu}{G} P_0^2 \int dk k h_k^{(1)} e^{ikx}. \tag{34}$$

Inserting this expression into the interfacial evolution equation (4) and assuming an exponential growth $h^{(1)}{}_k = \exp(\omega t)$, we obtain that the growth rate is

$$\omega = M\mathcal{V}_0 \frac{(1-\nu)P_0^2}{G} k^3. \tag{35}$$

The above dispersion relation implies that the interface is unstable due to mass diffusion under a normal load. That being said, the only difference, to the viscous-solid system presented in the previous section, is that when the viscous layer is at rest, the stabilizing shear stress is no longer present. It should therefore be emphasized that the boundary conditions are quintessential for the stability of the interface. Note that a similar setup with finite size elastic bulk parts has been studied recently in *Bonnetier et al.* [2009]. Here, a minimum energy criteria and variational calculus for shape perturbations were employed and revealed along the lines of the above calculation that the interface is linearly unstable when the fluid is at rest and for wave number smaller than the surface tension cutoff.

5. Discussion

5.1. Grain-Grain Contacts

[19] If the viscous layer separating the two solid materials is removed such that we have perfect stress transmission at the interface and the system can undergo dry recrystallization (i.e., we have a transport of mass across and normal to the interface), then the morphological stability of the interface depends on the complete set of material parameters of both solid phases. The corresponding stability diagram in this case becomes slightly more complex. In a previous work [*Angheluta et al.*, 2009], we have considered the dynamics of dry recrystallization between stressed solids. Similar to the derivations carried out for the solid-viscous layer system, the rate of mass transport across the interface is proportional to the gradients (jump) in the local chemical potential. In general, it turns out that contrasts in referential densities of the two solids often lead to the formation of fingerlike structures aligned with the principal direction of the far-field stress. In cases where the referential densities are identical the stability depends on the "compressibility" of the material. Like for the viscous-solid system, Poisson's ratio plays a crucial role in the stability.

5.2. Slow Displacements on Faults

[20] Most large earthquakes are followed by postseismic deformation, which can last for several years. Such deformation is usually thought to be localized directly on the rupture plane and often described as afterslip whose amplitude could be equivalent to coseismic slip (see *Pritchard and Simons* [2006] for a review). Such slow slip is also related to the increase of the elastic wave velocity in the fault zone after an earthquake [*Brenguier et al.*, 2008]. The slow relaxation of the fault is interpreted as the creation of new solid-solid contacts, related to an increase of the cohesion of the fault material. In the present study, we propose that the small roughness evolution of a fault plane by a dissolution precipitation instability could be a possible mechanism to explain observations of fault healing processes. Indeed, in fault zone, the state of stress is such that the ratio between the shear stress σ_{nt} and the normal stress σ_{nn}, which defines the friction coefficient $\mu_s = \frac{\sigma_{nt}}{\sigma_{nn}}$, varies in a range [0.1–0.2] for weak faults to [0.6–0.8] for stronger seismic faults. In the present study, we have demonstrated that the transition from stability to instability depends on Poisson's ratio such that if $\mu_s \leq \sqrt{\frac{1-\nu}{2}}$ the interface is unstable. For typical crustal rocks ν varies in the range [0.2–0.4], indicating that the transition occurs for $\mu_s \leq$ [0.5–0.6] (i.e., for static friction coefficients smaller than those deduced for most strong faults).

[21] In Figure 3, we presented a stability diagram that relates the static friction coefficient with the morphological stability of the interface. It was seen that the interface, if the stress is close to the level of slip, in general would evolve by surface diffusion in such a way that $\mu_s \to \sqrt{\frac{1-\nu}{2}}$. However, the static friction coefficient μ_s may never evolve toward such a value, either because the time needed for surface diffusion is much larger than the characteristic time of stress build up and relaxation or because the system is always loaded far below the critical stress needed for slip.

[22] The striations shown on the fault plane of Figure 1 are due to several processes such as mechanical abrasion, gouge fragmentation, creation and destruction of fault topography during seismic slip, and healing during the interseismic period. The anisotropy of the surface comes from the fact that mechanical abrasion in the direction of slip creates grooves at all scales (in fact, high-resolution analyses of fault surface roughness demonstrate the presence of scaling relationships [*Renard et al.*, 2006; *Sagy et al.*, 2007]). Other studies have shown that the presence of large-scale bumps, perpendicular to the direction of slip, are interpreted as a viscous instability during seismic slip [*Sagy and Brodsky*, 2009]. In the present study, we focus on contact formation and restrengthening of the interface. Clearly such effect overlies other deformation processes and would be difficult to isolate using high-resolution topography measurements. However, the roughening restrengthening

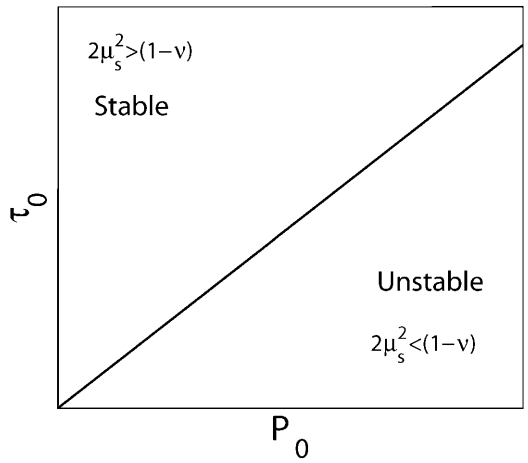

Figure 3. Stability diagram for a stressed interface. The interface is morphologically stable whenever $\tau_0 > \sqrt{\frac{1-\nu}{2}}P_0$ and unstable otherwise. The stability regions are separated by a neutral curve represented in the black solid line. The admissibility of certain regions is determined by the static friction coefficient μ_s, which sets a boundary between the maximum shear stress the system can sustain for a given normal load. In general, it is expected that the instability (stability) gives rise to an decrease (increase) in the friction coefficient. It is seen that if $\mu_s < \sqrt{\frac{1-\nu}{2}}$, the interface is morphologically unstable.

effect should be an important ingredient of the long-term evolution of active fault zone mechanical properties.

6. Conclusion

[23] Using an analytical approach we have shown that geological interfaces can be unstable under morphological perturbations when submitted to particular states of stress and when mass transfer is allowed across or along the interfaces. Previous studies have mostly considered the stability of interfaces of solid materials under compression, here we have analyzed systems where both a shear and compressive load is applied. Our analysis reveals an intricate relationship between the stability of a sheared interface and Poisson's ratio of the bulk material. In summary, we have shown that when a solid is in contact with a viscous layer at rest, the interface is always unstable for wavelengths larger than the critical length set by the surface tension. However, when the viscous layer flows or finite shear stresses are transmitted across the interface we observe that the interface becomes stable. It therefore follows that the stability of an interface is controlled by the ratio between the normal and shear load. We applied our analysis to the stability of faults and established a relationship between the static friction coefficient and Poisson's ratio. In general the faults interface corrugates in such a way that $\mu_s \rightarrow \sqrt{\frac{1-\nu}{2}}$. Further investigations (e.g., from field observations, to check this behavior are encouraged).

[24] **Acknowledgments.** We thank Ray Fletcher, Reinier van Noort, and Yanick Ricard for very useful discussions and comments, as well as the Associate Editor Reid Cooper. This project was supported by of Geological Processes, a Center of Excellence at the University of Oslo and by the *Agence National pour la Recherche* grant ANR-JCJC-0011-01.

References

Angheluta, L., E. Jettestuen, J. Mathiesen, F. Renard, and J. B. (2008), Stress-driven phase transformation and the roughening of solid-solid interfaces, *Phys. Rev. Lett.*, *100*, 096106.

Angheluta, L., E. Jettestuen, and J. Mathiesen (2009), Thermodynamics and roughening of solid-solid interfaces, *Phys. Rev. E*, *79*, 03601.

Asaro, R., and W. Tiller (1972), Interface morphology development during stress corrosion cracking: I. Via diffusion, *Met. Trans.*, *3*, 1789–1796.

Ben Zion, Y., and C.-G. Sammis (2003), Characterization of fault zones, *Pure Appl. Geophys.*, *160*, 677–715.

Bisschop, J., and D. Dysthe (2006), Instabilities and coarsening of stressed crystal surfaces in aqueous solutions, *Phys. Rev. Lett.*, *96*, 146103.

Bonnetier, E., C. Misbah, F. Renard, R. Toussaint, and J.-P. Gratier (2009), Does roughening og rock-fluid-rock interfaces emerge from a stress-induced instability?, *Eur. Phys. J. B*, *67*, 121–131.

Brenguier, F., M. Campillo, C. Hadziioannou, N. M. Shapiro, N. R. M., and E. Larose (2008), Post-seismic relaxation along the san andreas fault at parkfield from continuous seismological observations, *Science*, *321*, 1478–1481.

Cantat, I., K. Kassner, C. Misbah, and H. Müller-Krumbhaar (1998), Directional solidification under stress, *Phys. Rev. E*, *58*, 6027–6040.

de Meer, S., C. J. Spiers, and S. Nakashima (2005), Structure and diffusive properties of fluid-filled grains boundaries: An in-situ study using infrared (micro) spectroscopy, *Earth Planet. Sci. Lett.*, *232*, 403–414.

den Brok, S. W. J., and J. Morel (2001), The effect of elastic strain on the microstructure of free surfaces of stressed minerals in contact with an aqueous solution, *Geophys. Res. Lett.*, *28*, 603–606.

Dysthe, D., F. Renard, J. Feder, B. Jamtveit, P. Meakin, and T. Jøssang (2003), High resolution measurements of pressure solution creep, *Phys. Rev. E*, *68*, 011603, doi:10.1103/PhysRevE.68.011,603.

Ebner, M., D. Koehn, R. Toussaint, F. Renard, and J. Schmittbuhl (2009), Stress sensitivity of stylolite morphology, *Earth Planet. Sci. Lett.*, *277*, 394–398, doi:10.1016/j.epsl.2008.11.001.

Fletcher, R. A. (1973), Propagation of a coherent interface between two non-hydrostatically stressed crystals, *J. Geophys. Res.*, *78*, 7661–7666.

Gal, D., A. Nur, and E. Aharonov (1998), Stability analysis of a pressure-solution surface, *Geophys. Res. Lett.*, *25*, 1237–1240.

Ghoussoub, J., and Y. M. Leroy (2001), Solid-fluid phase transformation within grain boundaries during compaction by pressure solution, *J. Mech. Phys. Solids*, *49*, 2385–2430.

Gratier, J., P. Favreau, and F. Renard (2003), Modelling fluid transfer along californian faults when integrating pressure solution crack-sealing and compaction processes, *J. Geophys. Res.*, *108*(B2), 2104, doi:10.1029/2001JB000380.

Grinfeld, M. (1986), Instability of the separation boundary between a non-hydrostatically stressed solid and a melt, *Sov. Phys. Dokl.*, *31*, 831.

Grinfeld, M. (1992), On the morphology of the stress-driven corrugations of the phase boundary between the solid and its melt, *J. Phys. Condens. Matter*, *4*, L647–L652.

Kassner, K., and C. Misbah (1994), Nonlinear evolution of a uniaxially stressed solid: A route to fracture?, *Europhys. Lett.*, *28*, 245.

Koehn, D., F. Renard, R. Toussaint, and C.-W. Passchier (2007), Growth of stylolite teeth patterns depending on normal stress and finite compaction, *Earth Planet. Sci. Lett.*, *257*, 582–595.

Misbah, C., F. Renard, J.-P. Gratier, and K. Kassner (2004), Dynamics of a dissolution front for solids under stress, *Geophys. Res. Lett.*, *31*, L06618, doi:10.1029/2003GL019136.

Mullins, W. (1957), Theory of thermal grooving, *J. Appl. Phys.*, *28*, 333.

Muskhelishvili, N. I. (1953), *Some Basic Problems of the Mathematical Theory of Elasticity*, 3rd ed., Noordhoff, Groningen.

Paterson, M. S. (1973), Non-hydrostatic thermodynamics and its geological applications, *Rev. Geophys. Space Phys.*, *11*, 355–389.

Power, W.-L., T.-E. Tullis, S.-R. Brown, G.-N. Boitnott, and C.-H. Scholz (1987), Roughness of natural fault surfaces, *Geophys. Res. Lett.*, *14*, 29–32.

Power, W.-L., T.-E. Tullis, and J.-D. Weeks (1988), Roughness and wear during brittle faulting, *J. Geophys. Res.*, *93*, 15,268–15,278.

Pritchard, M., and M. Simons (2006), An aseismic slip pulse in northern chile and along-strike variations in seismogenic behavior, *J. Geophys. Res.*, *111*, B08405, doi:10.1029/2006JB004258.

Renard, F., J. Schmittbuhl, J. Gratier, P. Meakin, and E. Merino (2004), Three-dimensional structure of stylolites: roughness analysis, chemical measurements, and phenomenological modeling, *J. Geophys. Res.*, *108*, B03209, doi:10.1029/2003JB002555.

Renard, F., C. Voisin, D. Marsan, and J. Schmittbuhl (2006), High resolution 3d laser scanner measurements of strike-slip faults quantify its mor-

phological anisotropy at all scales, *Geophys. Res. Lett.*, *33*, L04305, doi:10.1029/2005GL025038.
Ricard, Y., J. Matas, and F. Chambat (2009), Seismic attenuation in a phase change coexistence loop, *Phys. Earth Planet. Inter.*, *176*, 124–131.
Sagy, A., and E. E. Brodsky (2009), Geometric and rheological asperities in an exposed fault zone, *J. Geophys. Res.*, *114*, B02301, doi:10.1029/2008JB005701.
Sagy, A., E. Brodsky, and G. Axen (2007), Evolution of fault-surface roughness with slip, *Geology*, *35*, 283–286.
Schmittbuhl, J., F. Renard, J. Gratier, and R. Toussaint (2004), The roughness of stylolites: Implications of 3d high resolution topography measurements, *Phys. Rev. Lett.*, *93*, 238501.
Schwartz, S., and J. Rokosky (2007), Slow slip events and seismic tremor at circum-pacific subduction zones, *Rev. Geophys.*, *45*, RG3004, doi:10.1029/2006RG000208.
Sekerka, R., and J. Cahn (2004), Solid-liquid equilibrium for non-hydrostatic stress, *Acta Mater.*, *52*, 1663–1668.
Shimizu, I. (1997), The nonequilibrium thermodynamics of intracrystalline diffusion under nonhydrostatic stress, *Philis. Mag. A*, *75*, 1221–1235.
Srolovitz, D. J. (1989), Surface morphology evolution in stressed solids: surface diffusion controlled crack initiation, *Acta Metall.*, *37*, 621–625.
Torii, R.-H., and S. Balibar (1992), Helium crystals under stress: the grinfeld instability, *J. Low Temp. Phys.*, *89*, 391–400.
van Noort, R., C. J. Spiers, and C. J. Peach (2007), Effects of orientation on the diffusive properties of fluid-filled grain boundaries during pressure solution, *Phys. Chem. Miner.*, *34*, 95–112.
Xiang, Y., and W. E. (2002), Nonlinear evolution equation for the stress-driven morphological instability, *J. Appl. Phys.*, *91*(11), 9414–9422, doi:10.1063/1.1477259.
Yang, W. H., and D. J. Srolovitz (1993), Cracklike surface instabilities in stressed solids, *Phys. Rev. Lett.*, *71*, 1593–1596.

L. Angheluta, J. Mathiesen, and F. Renard, Physics of Geological Processes, University of Oslo, Box 1047, N-0316 Blindern, Norway.
C. Misbah, LSP, University Joseph Fourier, Grenoble I, CNRS, BP 53, F-38041 Grenoble, France.
F. Renard, OSUG, LGCA, University Joseph Fourier, Grenoble I, CNRS, BP 53, F-38041 Grenoble, France.